3D Electrochemical-Mechanical Battery Simulation Tool: Implementation with Full Cell Simulations and Verification with Operando X-ray Tomography

Journal Article

Author(s):
Wenzler, Nils; Rief, Sebastian; Linden, Sven; Biebl, Fabian; Rütsche, Samuel; Glatt, Ilona; Streit, Anja; Zahn, Raphael; Fingerle, Mathias; Wood, Vanessa

Publication date:
2023-02

Permanent link:
https://doi.org/https://doi.org/10.3929/ethz-b-000601561

Originally published in:
Journal of the Electrochemical Society 170(2), https://doi.org/10.1149/1945-7111/acb5c9

Journal of The Electrochemical Society, 2023 **170** 020511

3D Electrochemical-Mechanical Battery Simulation Tool: Implementation with Full Cell Simulations and Verification with Operando X-ray Tomography

Nils Wenzler,[1] Sebastian Rief,[2] Sven Linden,[2] Fabian Biebl,[2] Samuel Rütsche,[1] Ilona Glatt,[2] Anja Streit,[2] Raphael Zahn,[1] Mathias Fingerle,[2] and Vanessa Wood[1,*,z]

[1]*Department of Information Technology and Electrical Engineering, ETH Zurich, Gloriastrasse 35, 8092 Zurich, Switzerland*
[2]*Math2Market GmbH, Richard-Wagner-Straße 1, 67655 Kaiserslautern, Germany*

Most commercially used electrode materials contract and expand upon cycling. This change in volume influences the microstructure of the cell stack, which in turn impacts a range of performance parameters. Since direct observation of these microstructural changes with operando experiments is challenging and time intensive, a simulation tool that takes a real or artificially generated 3D microstructure and captures the volumetric changes in a cell during cycling would be valuable to enable rapid understanding of the impact of material choice, electrode and cell design, and operating conditions on the microstructural changes and identification of sources of mechanically-driven cell aging. Here, we report the development and verification of such a 3D electrochemical-mechanical tool, and provide an example use-case. We validate the tool by simulating the microstructural evolution of a graphite anode and a $Li(Ni,Mn,Co)O_2$ cathode during cycling and comparing the results to X-ray tomography datasets of these electrodes taken during cycling. As an example use case for such a simulation tool, we explore how different volumetric expansion behaviors of the cathode material impact strain in the cell stack, illustrating how the material selection and its operation impact the mechanical behavior inside a cell.
 [DOI: 10.1149/1945-7111/acb5c9]

Manuscript submitted December 28, 2022; revised manuscript received January 20, 2023. Published February 23, 2023.

Supplementary material for this article is available online

With the widespread adoption of lithium-ion batteries (LIBs), prolonging their cycle life has become a key research focus. 3D imaging and electrochemical modeling on 3D reconstructions has highlighted the importance of microstructure on cell performance.[1–6] At the same time, most active materials used in commercial cells exhibit some volume change upon cycling. For example, graphite has a highly anisotropic expansion of up to 10.5%[1,7] and $LiNiMnCoO_2$ (NMC) exhibits a non-isotropic expansion and contraction.[8–10] The contraction is particularly dramatic for delithiation above ∼70% (high voltage operation) and leads to large stresses and subsequent cracking of the cathode particles.[10,11] These changes at the particle-level in turn drive dynamic changes to the microstructure of the electrode during cycling. Operando tomography has shown that for a high porosity graphite electrode under minimal pressure within a cell, the microstructural changes are on the same order as spatial inhomogeneities caused by manufacturing.[1] This change in microstructure can influence the transport properties and lead to inhomogeneity in charge distribution, local potential differences and with that e.g. more favorable conditions for lithium plating.[1.,12.,13.] Thus, understanding the mechanical changes is crucial for understanding the sources for accelerated degradation.

Such simulations must be done on realistic microstructures. For example, Lim et al. found up to 45% to 410% higher stresses in realistic particles than in models using idealized spherical particles.[14] However, microstructurally resolved electrochemical-mechanical models typically use finite element methods,[14–17] and meshing large structures, such as representative cell stacks consisting of an electrode a separator and another electrode, is computationally expensive and quickly becomes prohibitive. State-of-the-art finite volume methods that do not require mesh generation allow the use of large datasets, such as those produced by X-ray tomography (XTM) or focused ion beam scanning electron microscopy (FIB-SEM).[18] The numerical solver BESTmicro has become a widely used 3D volumetric electrochemical simulation tool based on such methods.[19,20] Math2Market has incorporated BESTmicro into the BatteryDict module of the scientific software GeoDict,[21] which offers a comprehensive suite of tools to import and process measured 3D image data, create realistic digital battery models, run simulations, and visualize results. Recently, Math2Market has implemented their in-house numerical solver BatteryLIR into GeoDict, which uses the same theory as BESTmicro but enables simulation on much larger, representative volumes in short runtimes compared to BESTmicro. The BatteryLIR solver allows an electrochemical simulation on battery microstructures of more than 1000^3 voxels on a standard workstation with 32 cores and 128 GB RAM. This performance is necessary to handle the microstructures investigated in this study. Furthermore, the GeoDict software provides 3D mechanical simulations using the FeelMath numerical solver developed by Fraunhofer ITWM.[22,23]

In this work, we develop and validate a new module that combines the electrochemical simulation (BatteryLIR) and the mechanical simulation (FeelMath). The operation and functionality of the resulting module is illustrated in Fig. 1. A 3D microstructure is loaded and material parameters are assigned to each phase, including standard electrochemical (e.g. open circuit potential U_0 and maximum lithium concentration c_{max}) and mechanical (e.g. Young's Modulus and Poisson Ratio) parameters as well as a coefficient of expansion vs lithium concentration (Table A-1). Based on the lithium concentration distribution calculated from electrochemical simulations (Fig. 1b), the expansion is computed. From this, the displacement, stress, and strain distributions are computed (Fig. 1c). On the new, mechanically deformed structure, a new electrochemical simulation can be performed. Here, we verify the implementation by comparing the simulated expansion of two different electrode structures to reconstructions of the same electrode imaged with X-ray tomography during cell cycling (*operando tomography*). Having verified the simulation tool, we then demonstrate how it can be used to simulate and analyze the expansion behavior of a complete LIB electrode stack and compare the influence on the cell stack of two different cathode expansion behaviors.

*Electrochemical Society Member.
[z]E-mail: wood@ethz.ch

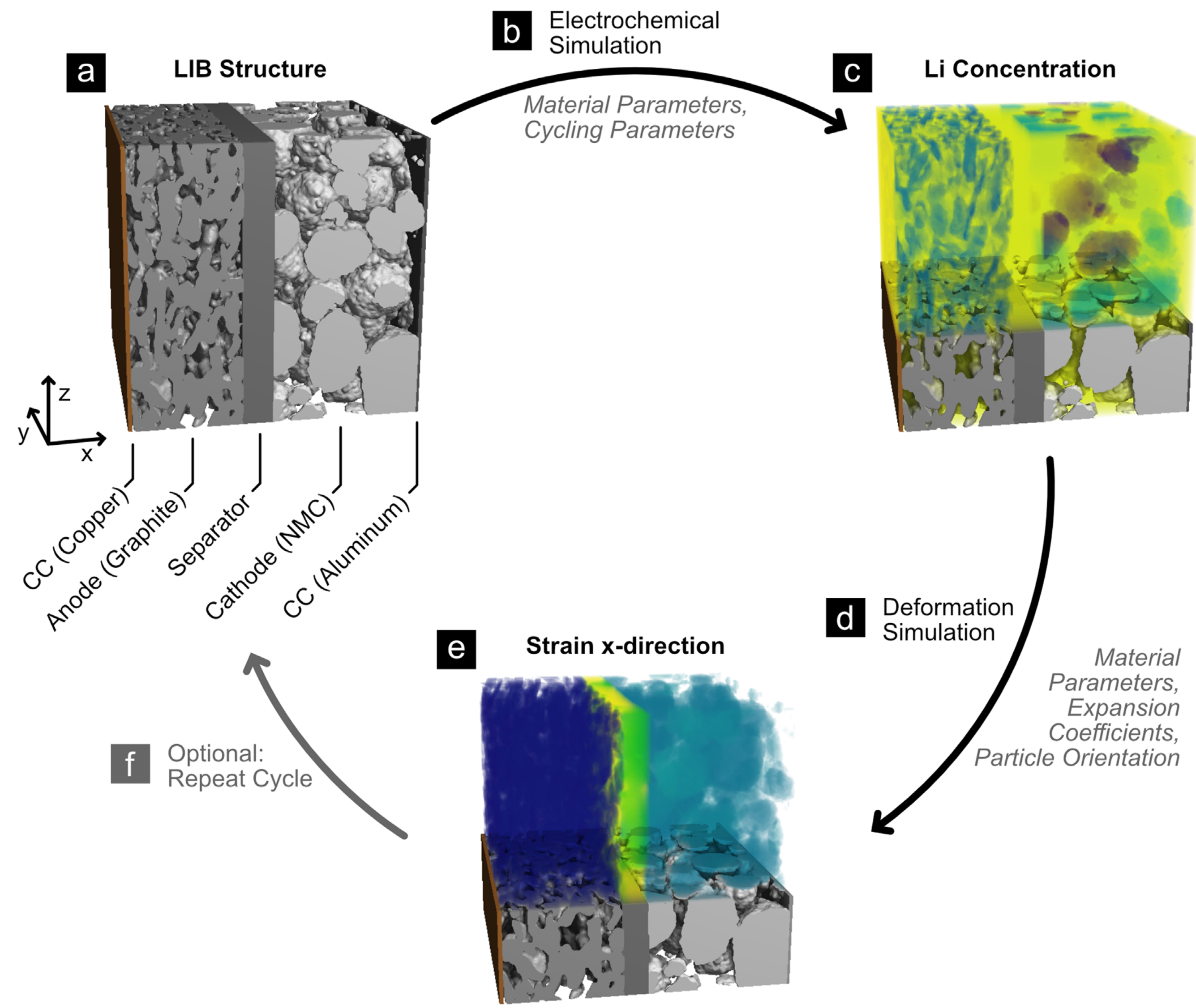

Figure 1. 3D electrochemical-mechanical battery simulation tool. The developed simulation tool combines 3D electrochemical and mechanical modeling and allows simulation of full-cell stacks with microstructural resolution. (a) The battery structure is digitally assembled from the measured or artificial electrode volumes. After parametrization of the materials and specification of the cycling protocol, the electrochemical behavior of the entire cell is simulated (b). Based on calculated distribution of lithium concentration within the cell at different time steps (c), the expansion coefficient is used to compute the stress and strain (d), (e). Using the deformed structure subsequent (dis-)charge cycles can be simulated (f).

Experimental

Simulation tool.—To simulate the volumetric changes during charging and discharging, a coupling between electrochemical and mechanical numerical simulation is developed and implemented into the commercial scientific software GeoDict—The Digital Material Laboratory.[21]

BatteryDict uses measured or artificial microstructures. Measurements can be imported already labeled or as raw data, using the segmentation tools included in GeoDict to separate phases and particles. Alternatively, a range of tools are provided to generate artificial microstructures and to add phases (e.g. carbon black binder (CBD)).

The GeoDict module BatteryDict runs the BatteryLIR solver (based on the theory of the BESTmicro solver developed at Fraunhofer ITWM[19,20]), which performs an electrochemical simulation, computing the local lithium concentration, potentials, overpotentials, ionic and electronic current densities and diffusion flux as function of time.

For the new module, each active material in the digital battery microstructure is assigned one (isotropic) or two (anisotropic) expansion coefficients. These coefficients relate the lithium concentration to the expansion in a linear fashion. The anisotropic behavior can be defined on a voxel level (requiring labeled particles with orientation information) or on an electrode level (all particles in the electrode are assumed to be aligned with one crystallographic direction in-plane).

The new module simulates the local volumetric changes (on a voxel level) based on the local lithium concentration difference and computes local stress, strain, and displacement. This mechanical simulation is implemented based on the FeelMath solver developed at Fraunhofer ITWM.[22,23]

This coupled electrochemical-mechanical functionality has been incorporated in the beta version of the BatteryDict-Degradation module, which is available for purchase and is marketed by Math2Market GmbH as an add-on module. It requires the GeoDict modules BatteryDict with the BatteryLIR solver and ElastoDict-LD with the FeelMath solver. The computational minimum requirements are a standard workstation with 16 cores and 128 GB RAM.

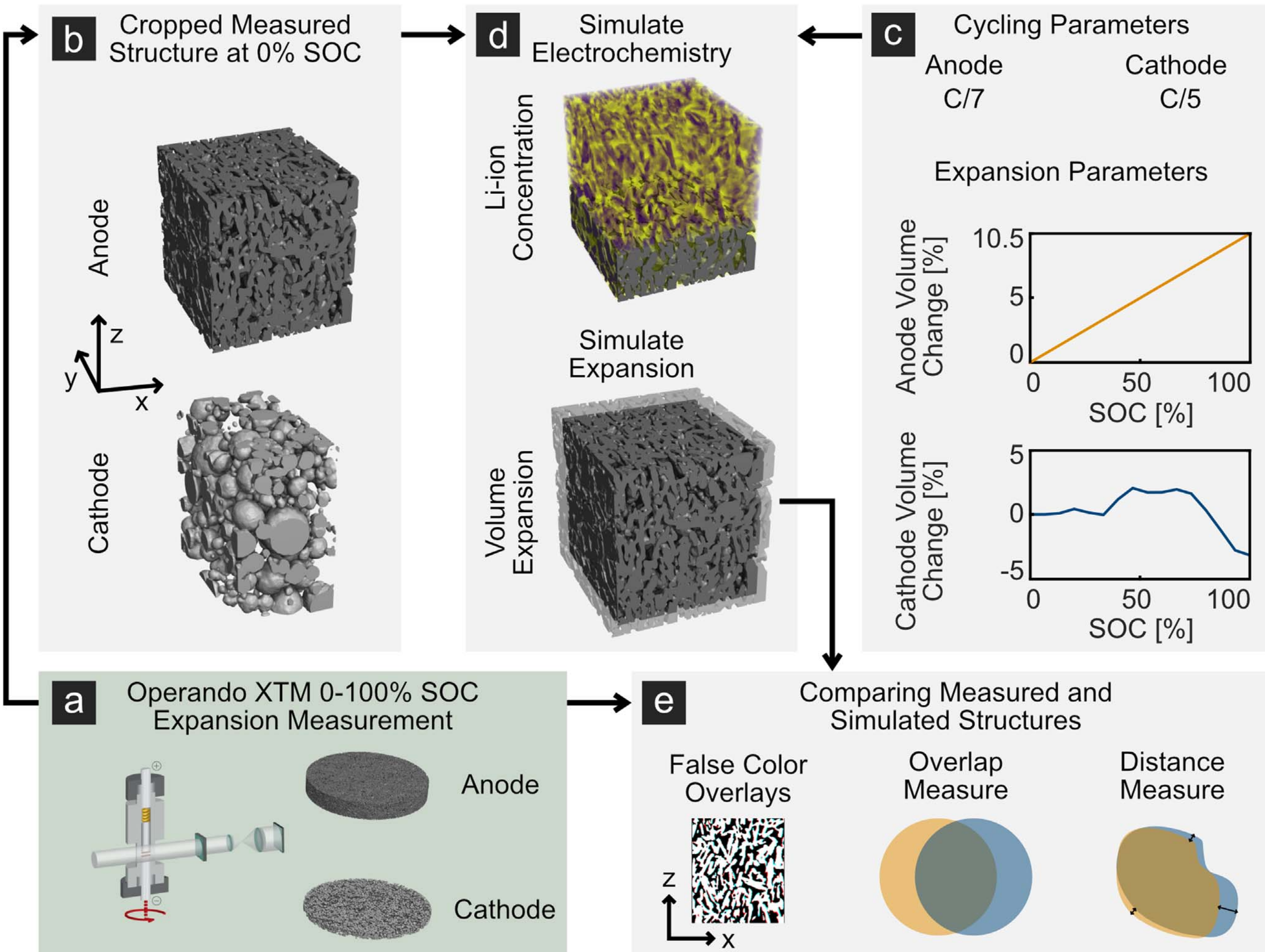

Figure 2. Verification procedure. (a) Operando X-ray tomographic microscopy (XTM) is used to track the anode and cathode during cycling. (b) Reconstructions of the initial cathode and anode volume (i.e., taken at 0% SOC) are then imported into the simulation tool. (c) Anode and cathode expansion coefficients are taken from experiment. (d) Electrochemical and mechanical simulations are performed with the module to match XTM measurements conditions (e.g., C/7 and C/5). (e) To verify the simulation tool, we compare the simulation results and the XTM operando measurement at different SOC, using an overlap measure (Dice) and a distance measure (average Hausdorff distance) as the quantification parameters.

Current limitations to the module.—For completeness, here we discuss limitations to the current implementation of the electro-chemical-mechanical coupling and the restrictions this places on this study.

First, due to the implementation of the expansion coefficient as a linear factor, a non-linear expansion can currently only be implemented by calculating each point on the non-linear expansion curve with respect to 0% SOC. This means that there is no error propagation as every step is calculated relative to the original volume. Furthermore, if a material both expands and contracts (e.g. NMC811) in one cycle, it limits interpretability of stress results as the resulting stress is not calculated from the already expanded or contracted structure but the original one.

Second, the mechanical solver does not account for the formation of new contacts between particles during one step of the computation. This means that stresses arising from two particles touching during one step are not accounted for. In addition, previously touching voxels cannot detach, which can lead to locally unrealistic stresses and currently complicates the simulation of effects like friction or sliding.

Third, the BatteryDict-Degradation beta-version is currently implemented such that electrochemical simulations can effectively only be performed for one charge or discharge cycle and subsequently the deformed microstructure is calculated based on the lithium concentration fields at the different SOC of interest. This means that the deformation currently does not influence the electrochemical simulation within one cycle. Thus, microstructural changes (e.g. porosity and tortuosity) only take effect in the next cycle. A coupling over many cycles and/or coupling over several charging or discharging steps during a cycle is under development.

Fourth, there are currently only two boundary conditions options for the mechanical simulation: *Confined* and *Free*. To study realistic cell designs and to study the influence pressure has on the cell stack, boundary conditions that allow user defined pressures would be ideal.

Despite these current limitations, the module enables the study of particle volume changes during cycling and it is especially useful to study the interplay of the electrodes in a full cell and the influence of different expansion parameters on the individual cell components. Furthermore, development work to address the discussed limitations will be intensively pursued for the release version of the module and for subsequent product releases.

Verification.—To validate the module, we compare the simulation results to operando XTM measurements of 1) a graphite anode during lithiation and 2) a $LiNi_{0.8}Mn_{0.1}Co_{0.1}O_2$ (NMC811) cathode during delithiation. Figure 2 depicts the verification of the simulation using two operando XTM measurements.[1]

A sub-volume measuring 256 × 256 × 244 voxels for the anode and 256 × 256 × 150 voxels for the cathode is simulated. The edge

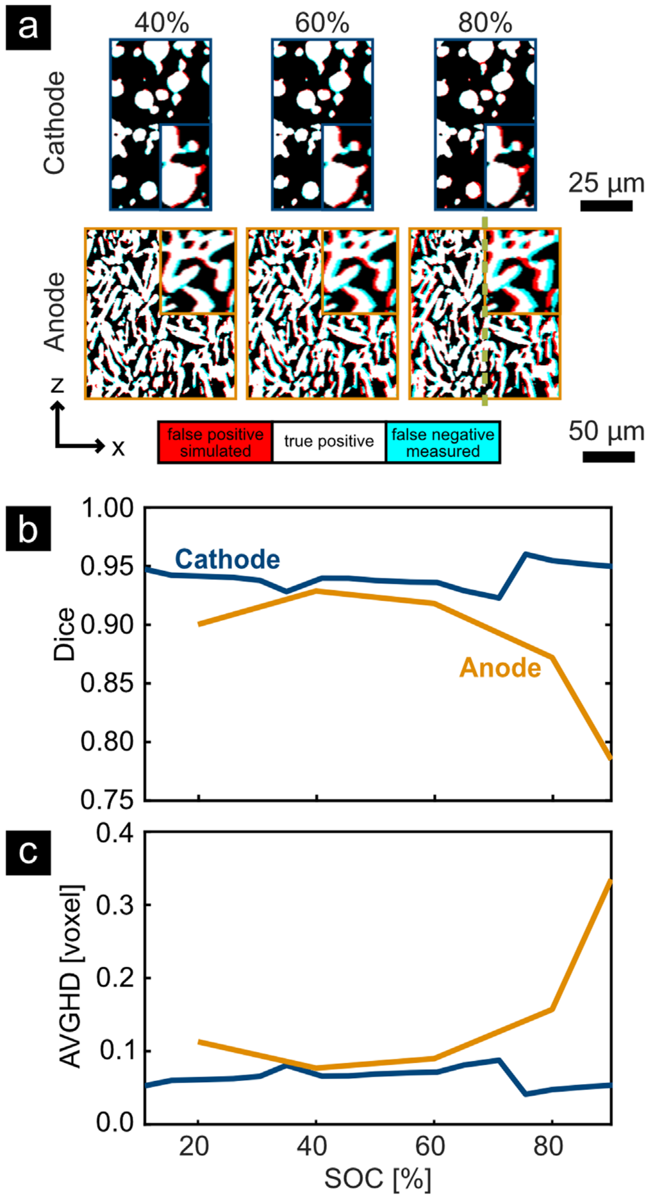

Figure 3. Verification of simulation the tool. (a) Overlays of 2D cross sections of the simulated and imaged electrodes (cathode top and anode bottom) at 40, 60, and 80% state-of-charge (SOC). The pore space is shown in black. White voxels indicate where the simulation agrees with the measurement. Red coloring indicates where the simulation incorrectly shows the presence of a particle, while blue indicates where the simulation has underestimated particle expansion or has failed to capture particle motion. The agreement between simulation and experiment for the anode (yellow line) and cathode (blue line) is quantified by (b) the Dice value and (c) the average Hausdorff distance (AVGHD).

length of the voxels is 0.65 μm and 0.325 μm for anode and cathode, respectively.

For the cathode microstructure, the NMC811 phase is segmented and modeled with isotropic expansion, with the particle expansion parameters extracted directly from XTM measurements. Expansion in graphite is anisotropic. Ideally, the individual graphite particles could be individually segmented and labeled so that their orientation could be identified. However, due to limitations in contrast and resolution of the anode operando XTM measurement, the reconstructed volumes are only segmented into graphite and pore space phases. Since most particles lie with their major x-axis parallel to the current collector,[1,7,24,25] we model the anode with a global anisotropic expansion behavior. The total expansion is set to 10.5% with 7.5% in the through-plane direction (x) and 2.75% in the in-plane direction (y-z). The latter two values have been determined empirically by a parameter sweep and finding the best match with the measurement (Fig. B-1).

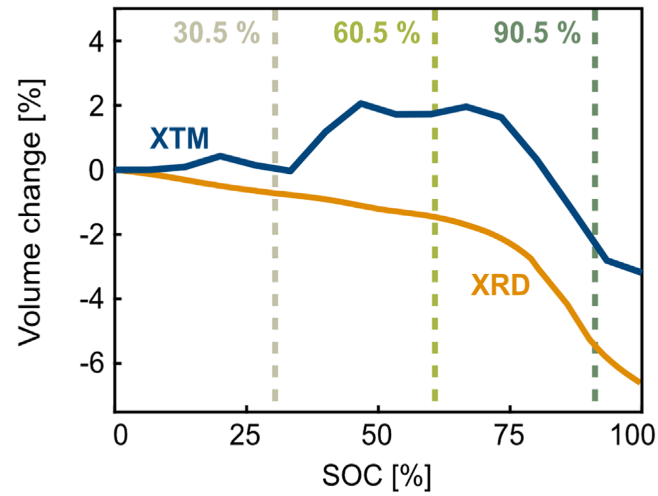

Figure 4. Expansion behaviors. Two different expansion behaviors for the NMC811 cathode and their influence on the full cell stack are compared. One expansion behavior is extracted from the operando X-ray tomography (XTM) data and describes the average expansion behavior of NMC811 particles in the first cycle, charged to 4.6 V. The other expansion behavior describes the unit cell volume change over the same cycle, measured with operando X-ray diffraction (XRD).[27] Dashed lines indicate three different states-of-charge (SOC) (30.5%, 60.5%, 90.5%).

Anode volumes are calculated stepwise for five SOCs, 20%, 40%, 60%, 80% and 90%. Due to the non-linear nature of the NMC811 expansion (see section on limitations above), the expansion is calculated from 0% SOC to each of 17 SOC values between 11% and 90.5% (0% to 11%, 0% to 15.5%, …, 0% to 90.5%) individually.

The boundary conditions for the expansion are set to *Free*, meaning mechanically unconstrained, as this best matches the measurement (Fig. B-1). For both electrodes, the simulated c-rate is matched to the measurement c-rate. In GeoDict, *Graphite* and *NMC333* are used as materials for anode and cathode respectively with all parameters other than expansion coefficient left on their default setting. Table A-2 lists all used material parameters.

To compare the measured and the simulated volumes, an alignment in the electrode through-plane has to be performed to correct for different expansion centers. The measured sample is a cut out of a larger volume that is fixed on one side, whereas the simulation expands from the center of the simulated volume. The correction is done by finding the highest slice correlation when shifting the two volumes relative to each other and is performed with Matlab. As a result, the final compared volumes are slightly cropped.

The quality of the simulation is then evaluated using both the Dice value and average Hausdorff distance.[26]

Full electrode stack.—The full electrode stack is built from the two electrodes used for the verification, with the cathode down sampled to match the anode voxel edge length of 0.65 μm. The anode and cathode thicknesses are set to 100 voxels (120.25 μm) and 135 voxels (87.75 μm), respectively, such that the cell is balanced. The material parameters are the default values provided by GeoDict (see Table A-2).

The separator is 27 voxels (17.55 μm) in thickness. It is modeled as a "Separator" in the electrochemical simulation: This means, that the ionic transport properties of the electrolyte phase are used, modified by an effective factor which accounts for the tortuosity of the separator microstructure. For the mechanical simulation, the elastomechanical parameters are set to match those of an electrolyte-

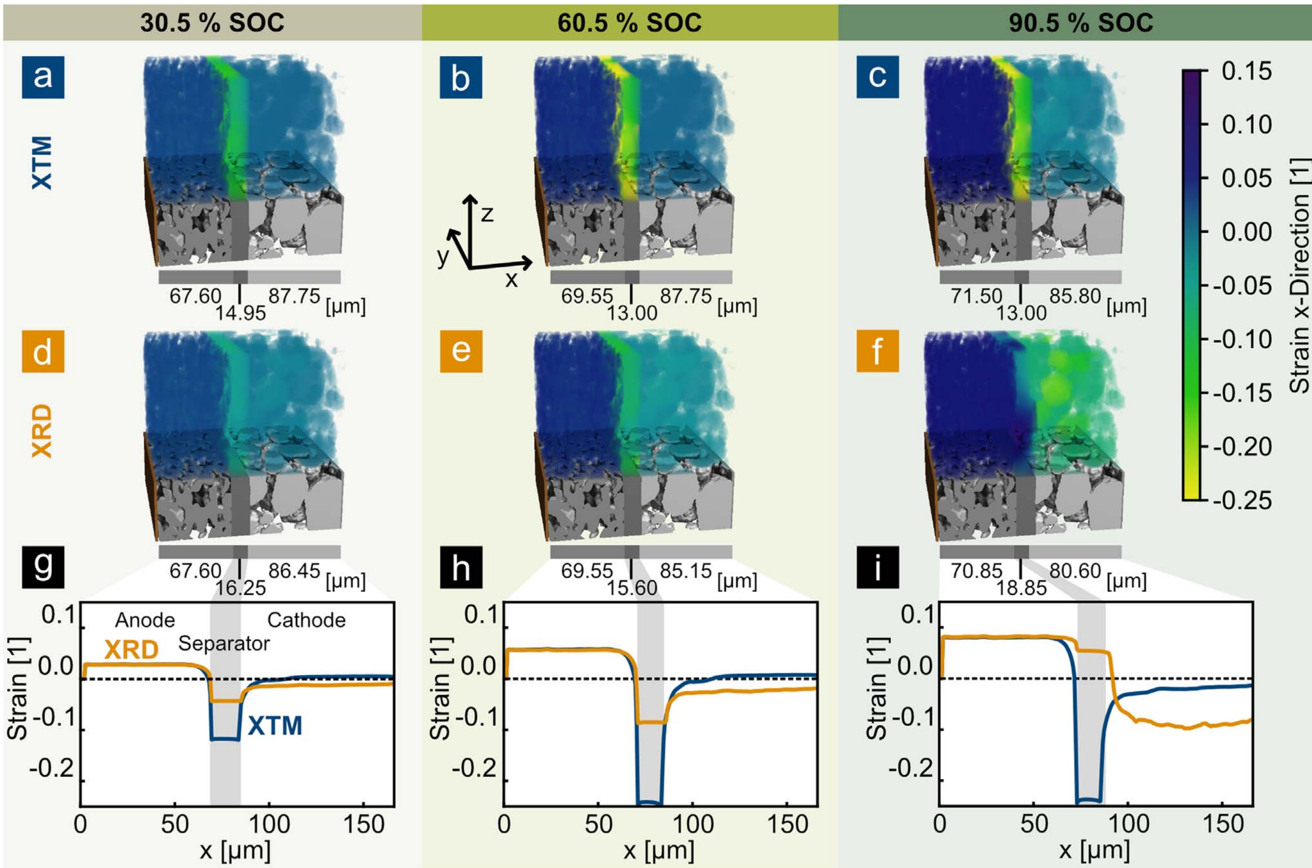

Figure 5. Strain in the full cell. The x-direction strain distributions are shown for the XTM parameters (**a**)–(**c**) and the XRD parameters (d)–(f) for three different SOC. (g)–(i) The average strain for every y-z-slice in x-direction for both the XTM-based expansion coefficients (blue line) and the XRD-based expansion (orange line).

immersed porous membrane (Young's modulus of 1.08 MPa and a Poisson's ratio of 0).[13] The copper and aluminum current collectors are fixed in size (3 Voxels, 1.95 μm).

Full stack simulations are performed two times at a rate of C/5 using two different sets of expansion parameters. For the first simulations, the same expansion parameters from the verification are used for both anode and cathode. For the second simulation, the crystal unit cell volume expansion is given as the expansion parameter for the cathode. Table A-3 lists all cycling parameters used for the simulations and the electrochemical results are shown in Fig. B-2.

Verification of the Simulation Tool

Figure 3 presents the results of the verification. The false color overlays of 2D slices through the simulated electrode and the binarized XTM images visualize the agreement (Fig. 3a). To quantify this agreement, two metrics are used. The Dice value (Fig. 3b) measures the degree of spatial overlap between two objects, where a value of 1 corresponds to complete overlap and 0 to no overlap. The Dice value is insensitive to the shape of the particle. The average Hausdorff distance (AVGHD, Fig. 3c), on the other hand, is a distance measure that is sensitive to differences in shapes of the two compared images.[26] The value indicates an average distance in voxels, with 0 being perfect overlap.

For the anode (yellow line in Figs. 3b and 3c), both the Dice value and the Hausdorff distance show decreasing agreement for higher SOC. This is in line with our expectations. Since we do not segment the individual particles of the anode and apply a global expansion to the graphite phase instead of to the individual particles, the agreement between simulation and experiment decreases with increasing volume change (i.e., higher SOC).

For the cathode, the Dice value is >0.90 and the AVGHD is <0.1 across the entire SOC range. This high level of agreement between the simulation and XTM is expected given that: 1) the isotropic particle expansion information is extracted from the same XTM measurement and 2) the cathode expansion is calculated relative to 0% SOC for each point, so there is no error propagation. The latter also explains the increase in similarity at ~75% SOC. At this point, the volume change relative to fully lithiated is zero (NMC811 first expands and then contracts), the simulated change in volume and therefore the resulting errors are small. The small deviations between simulation and experiment mainly stem from details at the resolution limit, such as attachment or detachment of smaller particles adjacent to bigger ones, slightly different movement of the particles in measurement and simulations as well as from residual error from the different centers of expansion. The latter source of error stems from the fact that only unconstrained or fixed boundary conditions are implemented, whereas a variable pressure boundary condition would be more realistic, especially in the through plane direction. We achieved the best overall match to experiment using unconstrained boundary conditions (Fig. B-1), which is reasonable as the specialized cells used for the XTM measurements do not constrain the electrode as strongly as a commercial cell.[1] These unconstrained boundary conditions however allow greater displacement of the particles away from the center point of the electrode than actually is possible in a cell. Since the majority of the expansion is in the through-plane direction (x-axis), the mismatch is highest along this axis (see false color overlay in Fig. 3a).

In summary, these two scenarios show that different implementations of the software result in good performance of the simulated tool. The example of the graphite anode points to the benefit of segmenting the individual particles and applying the volume change

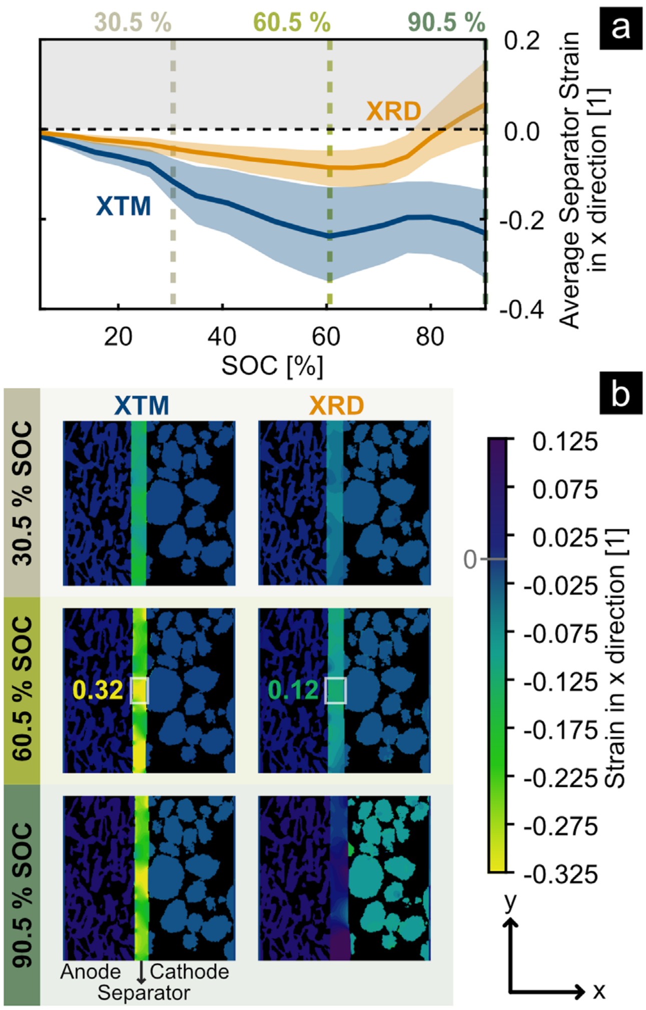

Figure 6. Strain in separator. (a) The average strain in the separator in x direction is plotted against the SOC. The shaded area indicates the 5th to 95th percentile of all strain values in the separator (i.e. the spread, excluding the 5% lowest and highest strain values). (b) Plot of the strain on cross-sectional slices through the cell showing that high strain in the separator occurs locally directly adjacent to NMC811 particles.

vs degree of lithiation directly. As a next step in the development of the code, implementation of boundary conditions that allow user defined pressures to be applied on the cell stack will be pursued.

Effect of Cathode Expansion Behavior On Full Cell Stack

As an application example, we select two different NMC811 particles expansion behaviors (Fig. 4) and explore their impact on a graphite-NMC811 cell stack. The first expansion behavior is the unit cell volume change measured using operando X-ray diffraction (XRD). The second is the volume change of the NMC811 particles measured using operando X-ray tomography (XTM) over the first charge of the cell (first delithiation of the cathode).[27]

Figure 5 shows the x-direction strain distributions with voxel resolution for three different SOCs (30.5%, 60.5%, and 90.5%) with the XTM-based expansion coefficient for NMC811 (Figs. 5a–5c) and with the XRD-based expansion coefficient for NMC811 (Figs. 5d–5f). The corresponding stress, lithium and potential distributions can be found in the Supporting Information (Figs. B-3, B-4). Figures 5g–5i show the average x-direction strain of each y-z-slice.

In the case of the XTM-based expansion parameter for the NMC811, the anode and the cathode both expand over the first charge cycle until ~70% SOC. This leads to compression of the separator (Figs. 5a–5b, 5g–5h, and 6a). This is expected since the separator (Young's Modulus E = 1.08 MPa) is softer than the graphite anode (E = 32 GPa) or NMC811 cathode (E = 200 GPa). From 60.5% SOC on, the separator regains some of its volume because the cathode contracts more than the anode expands. From ~80% SOC, on the cathode does not contract strongly and the separator undergoes further compressive strain caused by the anode expansion.

For the XRD-based expansion parameter for the NMC811, the cathode particles contract while the anode particles expands. The linear expansion of the anode is partly matched by the contraction of the cathode up to ~75% SOC, with the separator experiencing a small amount of compressive strain (<10%). Above ~75% SOC, the cathode contraction is larger than the anode expansion. In the simulation, this leads to the unrealistic result of the separator experiencing tensile strain (being stretched); in reality, the electrodes (i.e., boundary conditions) would not be fixed but the cell would always be kept under some minimum pressure. Or, in the case of fixed boundaries, these conditions would lead to the detachment of the NMC811 particles from the separator, an effect which currently cannot be simulated.

The difference in the separator compression found between the XTM and XRD parameter set highlights the impact particle expansion behavior can have on performance of a cell. For compressive strains of 5%–10% (as found for the XRD-based NMC811 parameters (Fig. 6b)), the porosity of a Polyethylene separator decreases 12.5%−20% (i.e., from 40% to 35% and 32% porosity). At compressive strains of 20%–40% (as found for the XTM-based NMC811 parameters), the porosity decreases 37.5%–60% (i.e. from 40% to 25% and 14% porosity). In the latter scenario, the transport properties are strongly impacted with large overpotentials steaming from descreased lithium ion conductivity though the separator (50 mV at 2 C for 20% compressive strain and over 50 mV already at 0.5 C for 40% compressive strain). Such overpotentials can push a cell out of safe cell operations.[13,28–30]

Conclusions

We successfully implemented and verified a coupled electrochemical-mechanical simulation that works on microstructures. The tool can be configured with a range of materials and can simulate half-cell or full-cell stacks. The example here using two different expansion parameters for NMC811 particles and the impact this has on the strain distributions in the cell, specifically the separator, highlights the importance of considering the volume change experienced by the particles during cell design. The example also highlights that in the case of polycrystalline or secondary particles composed of many individual grains, where expansion at the unit cell level leads to more dramatic morphological changes within the individual particles themselves (e.g., increase of internal porosity or fracture), using the unit-cell expansion on the particle phase, may not be sufficient to capture the complexity of the particle volume change.

In its current implementation, there are some limitations to the tool, mainly concerning boundary conditions and non-linear expansion behaviors. However, development work is ongoing to implement boundary conditions that allow user defined pressures. A future goal is the implementation of non-linear expansion behavior.

More fundamentally, it is important to recognize that this tool looks at the impact of the expansion or contraction of particles on the microstructure of the electrode and the strain in the different cell layers. The carbon-black and binder domain or the separator structure also undergo morphological changes due to the expansion behavior,[12,13,31] but the nanoscale porosity is implemented as an effective parameter. As presented in this work through the example of strain in the separator and its potential impact on the electrochemistry, it is also important to understand the impact of strain on these smaller nanoscale features. From a computation point of view, it is not realistic to include the actual nanoscale features. However, using representative microstructures it is possible to compute the transport parameters as a function of strain. These parameters can then in turn be used to parameterize such phases with effective transport parameters as a function of simulated strain, allowing these crucial changes of the transport parameters to be included in the simulation.

The long-term vision for BatteryDict-Degradation, including the features and improvements mentioned in this study, is to deliver a simulation platform for the prediction of degradation effects on the microscale for realistic battery cycling protocols and usage scenarios, improving the digital material design capabilities of GeoDict for batteries. On the mechanics side, damage models and models for crack propagation for different battery materials are of superior interest. Above that, electrochemical ageing phenomena like SEI formation and Li-plating will be implemented in the future.

ORCID

Nils Wenzler https://orcid.org/0000-0002-5713-8620
Vanessa Wood https://orcid.org/0000-0001-6435-0227

References

1. P. Pietsch et al., "Quantifying microstructural dynamics and electrochemical activity of graphite and silicon-graphite lithium ion battery anodes." *Nat. Commun.*, **7**, 1 (2016).
2. D.-W. Chung, M. Ebner, D. R. Ely, V. Wood, and E. García, "R. Validity of the Bruggeman relation for porous electrodes." *Model. Simul. Mater. Sci. Eng.*, **21**, 074009 (2013).
3. L. Zielke et al., "A Combination of X-ray tomography and carbon binder modeling: reconstructing the three phases of LiCoO 2 Li-Ion battery cathodes." *Adv. Energy Mater.*, **4**, 1301617 (2014).
4. E. Maire and P. J. Withers, "Quantitative X-ray tomography." *Int. Mater. Rev.*, **59**, 1 (2014).
5. J. R. Wilson, J. S. Cronin, S. A. Barnett, and S. J. Harris, "Measurement of three-dimensional microstructure in a LiCoO2 positive electrode." *J. Power Sources*, **196**, 3443 (2011).
6. P. R. Shearing et al., "Multi Length scale microstructural investigations of a commercially available Li-Ion battery electrode." *J. Electrochem. Soc.*, **159**, A1023 (2012).
7. T. Ohzuku, Y. Iwakoshi, and K. , Sawai, "Formation of lithium-graphite intercalation compounds in nonaqueous electrolytes and their application as a negative electrode for a lithium ion (shuttlecock) cell." *J. Electrochem. Soc.*, **140**, 2490 (1993).
8. W. Li, H. Y. Asl, Q. Xie, and , A. Manthiram, " Collapse of LiNi1- x- yCoxMnyO2 lattice at deep charge irrespective of nickel content in Lithium-Ion batteries." *J. Am. Chem. Soc.*, **141**, 5097 (2019).
9. A. O. Kondrakov et al., "Anisotropic lattice strain and mechanical degradation of high- and low-nickel ncm cathode materials for Li-Ion batteries." *J. Phys. Chem. C*, **121**, 3286 (2017).
10. T. M. M. Heenan et al., "Identifying the origins of microstructural defects such as cracking within ni-rich nmc811 cathode particles for Lithium-Ion batteries." *Adv. Energy Mater.*, **10**, 2002655 (2020).
11. P. Yan et al., "Intragranular cracking as a critical barrier for high-voltage usage of layer-structured cathode for lithium-ion batteries." *Nat. Commun.*, **8**, 1 (2017).
12. S. Müller et al., "Quantification and modeling of mechanical degradation in lithium-ion batteries based on nanoscale imaging." *Nat. Commun.*, **9**, 1 (2018).
13. M. F. Lagadec, R. Zahn, and V. Wood, "Designing polyolefin separators to minimize the impact of local compressive stresses on lithium ion battery performance." *J. Electrochem. Soc.*, **165**, A1829 (2018).
14. C. Lim, B. Yan, L. Yin, and L. Zhu, "Simulation of diffusion-induced stress using reconstructed electrodes particle structures generated by micro/nano-CT." *Electrochim. Acta*, **75**, 279 (2012).
15. Y. Zhao et al., "A review on modeling of electro-chemo-mechanics in lithium-ion batteries." *J. Power Sources*, **413**, 259 (2019).
16. L. Wu, X. Xiao, Y. Wen, and J. Zhang, "Three-dimensional finite element study on stress generation in synchrotron X-ray tomography reconstructed nickel-manganese-cobalt based half cell." *J. Power Sources*, **336**, 8 (2016).
17. L. Wu, Y. Wen, and J. Zhang, "Three-dimensional finite element study on li diffusion induced stress in fib-sem reconstructed LiCoO2 half cell." *Electrochim. Acta*, **222**, 814 (2016).
18. S. Linden, L. Cheng, and , A. Wiegmann, ". Specialized methods for direct numerical simulations in porous media." *Math2Market Tech. Rep.*, **1**, 6 (2018), All.
19. A. Latz and J. Zausch, "Thermodynamic consistent transport theory of Li-ion batteries." *J. Power Sources*, **196**, 3296 (2011).
20. A. Latz and J. Zausch, "Thermodynamic derivation of a Butler-Volmer model for intercalation in Li-ion batteries." *Electrochim. Acta*, **110**, 358 (2013).
21. Math2Market. GeoDict (Release 2022). (December 27, 2022).
22. M. Kabel, D. Merkert, and M. Schneider, "Use of composite voxels in FFT-based homogenization." *Comput. Methods Appl. Mech. Eng.*, **294**, 168 (2015).
23. H. Grimm-Strele and M. Kabel, "FFT-based homogenization with mixed uniform boundary conditions." *Int. J. Numer. Methods Eng.*, **122**, 7241 (2021).
24. P. Baade, M. Ebner, and V. Wood, "Rapid, non-invasive method for quantifying particle orientation distributions in graphite anodes." *J. Electrochem. Soc.*, **164**, E348 (2017).
25. H. Buqa, D. Goers, M. Holzapfel, M. E. Spahr, and P. Novák, "High rate capability of graphite negative electrodes for lithium-ion batteries." *J. Electrochem. Soc.*, **152**, A474 (2005).
26. A. A. Taha and A. Hanbury, "Metrics for evaluating 3D medical image segmentation: Analysis, selection, and tool." *BMC Med. Imaging*, **15** (2015).
27. N. Wenzler, "Characterization and simulation of mechanical transformations in lithium ion battery anodes and cathodes." *ETH Zurich* (2022).
28. J. Cannarella and C. B. Arnold, "The Effects of defects on localized plating in lithium-ion batteries." *J. Electrochem. Soc.*, **162**, A1365 (2015).
29. D. Lyu, B. Ren, and S. Li, "Failure modes and mechanisms for rechargeable Lithium-based batteries: a state-of-the-art review." *Acta Mech.*, **230**, 701 (2019).
30. Q. Wang, B. Mao, S. I. Stoliarov, and J. Sun, "A review of lithium ion battery failure mechanisms and fire prevention strategies." *Prog. Energy Combust. Sci.*, **73**, 95 (2019).
31. S. Müller et al., "Deep learning-based segmentation of lithium-ion battery microstructures enhanced by artificially generated electrodes." *Nat. Commun.*, **12**, 1 (2021).